NeuroImage 121 (2015) 243–252

Contents lists available at ScienceDirect

NeuroImage

journal homepage: www.elsevier.com/locate/ynimg

Heritability of the network architecture of intrinsic brain functional connectivity

Benjamin Sinclair [a,b,c,*], Narelle K. Hansell [c], Gabriëlla A.M. Blokland [c], Nicholas G. Martin [c], Paul M. Thompson [d], Michael Breakspear [c], Greig I. de Zubicaray [b], Margaret J. Wright [c], Katie L. McMahon [a]

[a] Centre for Advanced Imaging, University of Queensland, Brisbane, QLD 4072, Australia
[b] School of Psychology, University of Queensland, Brisbane, QLD 4072 Australia
[c] QIMR Berghofer Medical Research Institute, Brisbane, QLD 4029, Australia
[d] Imaging Genetics Center, Dept. of Neurology, Keck School of Medicine, University of Southern California, Los Angeles, CA 90095, USA

ARTICLE INFO

Article history:
Received 23 December 2014
Accepted 17 July 2015
Available online 28 July 2015

Keywords:
Resting state
Graph theory
Genetics
Heritability
Functional connectivity

ABSTRACT

The brain's functional network exhibits many features facilitating functional specialization, integration, and robustness to attack. Using graph theory to characterize brain networks, studies demonstrate their small-world, modular, and "rich-club" properties, with deviations reported in many common neuropathological conditions. Here we estimate the heritability of five widely used graph theoretical metrics (mean clustering coefficient (γ), modularity (Q), rich-club coefficient (ϕ_{norm}), global efficiency (λ), small-worldness (σ)) over a range of connection densities ($k = 5$–25%) in a large cohort of twins ($N = 592$, 84 MZ and 89 DZ twin pairs, 246 single twins, age 23 ± 2.5). We also considered the effects of global signal regression (GSR). We found that the graph metrics were moderately influenced by genetic factors h^2 ($\gamma = 47$–59%, $Q = 38$–59%, $\phi_{norm} = 0$–29%, $\lambda = 52$–64%, $\sigma = 51$–59%) at lower connection densities (≤15%), and when global signal regression was implemented, heritability estimates decreased substantially h^2 ($\gamma = 0$–26%, $Q = 0$–28%, $\phi_{norm} = 0\%$, $\lambda = 23$–30%, $\sigma = 0$–27%). Distinct network features were phenotypically correlated ($|r| = 0.15$–0.81), and γ, Q, and λ were found to be influenced by overlapping genetic factors. Our findings suggest that these metrics may be potential endophenotypes for psychiatric disease and suitable for genetic association studies, but that genetic effects must be interpreted with respect to methodological choices.

© 2015 Elsevier Inc. All rights reserved.

Introduction

There is growing evidence that the functional architecture of human brain networks has a profound influence on cognition and disease. The efficiency of information propagation in brain networks, or how far signals must travel to reach disparate parts of the network, has been shown to correlate significantly with intelligence (Li et al., 2009; van den Heuvel et al., 2009). The modularity of an individual's functional brain network, or the degree to which the network is partitioned into subnetworks (e.g., visual, sensory-motor, and default mode networks), can also predict performance on working memory tasks (Stevens et al., 2012). Further, almost all psychiatric diseases studied with neuroimaging have been characterized by departures from the established network architecture seen in healthy individuals (see Wang et al., 2010).

Even in the absence of a specific task or stimulus, fluctuations in the blood-oxygenation level dependent (BOLD) signal are correlated across the brain, revealing spatially distributed networks of coherent activity (Fox and Raichle, 2007), which overlap with task-related functional networks (Smith et al., 2009) and underlying structural networks (Damoiseaux and Greicius, 2009; Honey et al., 2009). Graph theory—a mathematical approach to study networks—has been applied to such resting state data (rs-fMRI) to measure higher order features of resting state networks (RSNs), such as efficiency and modularity (for a brief description of graph theory metrics, see Table 1, and Rubinov and Sporns, 2010 for a review). These features provide measures of the topological organization of brain networks, which have direct biological significance. Here we consider three measures of network segregation and community structure (γ, Q, ϕ_{norm}), a measure of network integration (λ), and a composite measure describing the trade-off between integration and segregation (σ).

Features showing strong heritability may be promising endophenotypes for neuropsychiatric disorders. More significantly, they may serve as targets for subsequent searches to identify particular sets

* Corresponding author at: Centre for Advanced Imaging, University of Queensland, Brisbane, QLD 4072, Australia.
E-mail addresses: b.sinclair@uq.edu.au (B. Sinclair), Narelle.Hansell@qimrberghofer.edu.au (N.K. Hansell), gabriellablokland@gmail.com (G.A.M. Blokland), Nick.Martin@qimrberghofer.edu.au (N.G. Martin), pthomp@usc.edu (P.M. Thompson), mjbreaks@gmail.com (M. Breakspear), Greig.dezubicaray@uq.edu.au (G.I. de Zubicaray), Margie.Wright@qimrberghofer.edu.au (M.J. Wright), Katie.McMahon@uq.edu.au (K.L. McMahon).

http://dx.doi.org/10.1016/j.neuroimage.2015.07.048
1053-8119/© 2015 Elsevier Inc. All rights reserved.

Table 1
Description of graph metrics. For a full review, see Rubinov and Sporns (2010).

Metric	Description	Mathematical definition
Mean clustering coefficient, $\boldsymbol{\gamma} = \frac{mC}{mC^{random}}$	The clustering coefficient describes the likelihood of two nodes that are connected to a common node being connected to each other. It is a measure of "cliquishness" in a network. To normalize, this probability is divided by the corresponding probability one would observe for a null hypothesis random network.	$mC = \frac{1}{n}\sum_{i\in N} C_i$ $C_i = \frac{2t_i}{k(k-1)}$ where t_i is the number of complete triangles around node i.
Modularity, Q	Modularity is the degree to which the network is partitioned into sub-graphs with a large number of connections within the sub-graphs, but relatively few connections between sub-graphs.	$Q = \sum_{u\in M}[e_{uu} - \sum_{v\in M} e_{uv}]$ where M is the set of modules, and e_{uv} is the proportion of links that connect nodes in module u with nodes in module v.
Rich-club coefficient, ϕ	ϕ quantifies the degree to which hubs (highly connected and/or central nodes) preferentially associate with each other. To normalize, this proportion is divided by the proportion that would be observed in a random network.	$\phi(k) = \frac{2E_{>k}}{N_{>k}(N_{>k}-1)}$ where $N_{>k}$ is the number of nodes with degree greater than k, and $E_{>k}$ is the number of links between those nodes.
Global efficiency $\boldsymbol{\lambda} = \frac{E_g}{E_g^{random}}$	Efficiency is the inverse of path length, where path length is the number of connections traversed to get from one node to another. This is averaged over all node pairs to give global efficiency. To normalize, the efficiency is divided by the efficiency one would observe in a random network.	$Eg = \frac{1}{n}\sum_{i\in N} E_i = \frac{1}{n}\sum_{i\in N}\frac{\sum_{j\in N} d_{ij}^{-1}}{n-1}$
Small-world index, $\boldsymbol{\sigma = \gamma\,\lambda}$	Small-world index describes how nodes in a network can be connected in relatively few steps, while maintaining local clustering. Complex networks generally have greater clustering than random networks, but comparable efficiency, giving them a greater small-worldness.	$\boldsymbol{\sigma = \gamma\,\lambda}$ $\boldsymbol{\lambda} = \frac{1}{\Lambda}$ where Λ is the harmonic mean of path length, i.e. the shortest number of links between two nodes.
Random network	Random networks provide null hypothesis reference networks to which the values of graph metrics can be compared. To create these networks, rewiring algorithms randomly reassign connections, a process which preserves low order features such as the connection density, number of nodes and degree distribution, while destroying higher order topological features such as clustering.	Random networks were generated using the Maslov and Sneppen (2002) algorithm, which preserves the degree distribution but not the weighted strength distribution. Rewiring was constrained to maintain full connectedness.
Degree	The degree of a node is the number of connections of that node	$K_i = \sum_{j\in N} a_{ij}$ Where a is the adjacency/connectivity matrix.

of influential genes, to better understand molecular mechanisms affecting intra-brain communication. Prior twin studies of RSNs suggest that cost efficiency (Fornito et al., 2011) and global efficiency (van den Heuvel et al., 2013) are moderately to strongly heritable (heritability, $h^2 = 60\%$ and 42%, respectively). However, both of these studies had small samples, examined different age groups (n = 58 and 86; ages 40 and 12; for Fornito et al. (2011) and van den Heuvel et al. (2013), respectively) and did not correct for nuisance covariates of global signal, white matter, and CSF. Heritability of graph measures of brain networks has also been observed with diffusion-weighted MRI (Dennis et al., 2011) and EEG (Smit et al., 2008).

We hypothesized that the common graph metrics of RSNs (γ, Q, ϕ_{norm}, $\boldsymbol{\lambda}$, and σ) calculated using a standard processing pipeline, would be moderately heritable and we examined the association between metrics and to what extent any association is due to a common genetic factor. As a network may vary according to the number of links, we estimated the heritability of each metric over a range of connection densities (k = 5–25%), as well as considering the effect of binarizing graphs. In addition, given the ongoing debate as to the inclusion of global signal regression (Murphy et al., 2009; Fox et al., 2009), we conducted our analysis both with and without GSR. We tested these predictions in a large cohort (N = 592) at approximately full brain maturation (mean age 23.5; e.g. Lebel et al., 2008).

Materials and methods

Participants

Adult twins were recruited as part of the Queensland Twin IMaging (QTIM) study (de Zubicaray et al., 2008), under approval of the Human Research Ethics Committees of the QIMR Berghofer Medical Research Institute, University of Queensland, and Uniting Health Care, Wesley Hospital. Written informed consent was obtained for each participant. Twins were scanned in the same session or within a week of each other. Participants were excluded if they reported any history of psychiatric disease, brain injury, substance abuse, or MR incompatibility.

Of the 619 participants with rs-fMRI data, 27 participants (including one twin pair) were rejected due to excessive head motion (translation > 3mm, rotation > 2°), image artifacts or observable neurological abnormalities (on visual inspection of images). The final sample consisted of 346 paired twins (84 monozygotic (MZ) pairs (61 female, 23 male) and 89 dizygotic (DZ) pairs (34 female, 13 male, 42 opposite sex)), and 246 unpaired twins, mean age 23.5 (±2.5), range 18–30. Zygosity was established using 9 independent polymorphic DNA markers, cross-checked with blood group and phenotypic data to give a greater than 99.99% probability of correct zygosity assignment (Wright and Martin, 2004). Zygosity was later confirmed by genome-wide single nucleotide polymorphism genotyping (Illumina 610 K chip).

Image acquisition

Imaging was conducted on a 4 Tesla Bruker Medspec whole body scanner

(Bruker). Participants were instructed to remain at rest with their eyes closed, and to not think of anything in particular and not fall asleep. The imaging sequence was a T2*-weighted gradient echo, echo planar imaging (GE-EPI) sequence (repetition time TR = 2100 ms; echo time TE = 30 ms; flip angle = 90°; field of view FOV = 230 × 230 mm, pixel size 3.6 × 3.6 mm, 36 coronal 3.0 mm slices with 0.6 mm gap, 150 volumes, total scan time 315 s). Prior to the rs-fMRI scan, a T1-weighted 3D structural image was acquired (MPRAGE, TR = 1500 ms; TE = 3.35 ms; inversion time TI = 700 ms; flip angle = 8°; FOV = 230 mm^3, pixel size 0.9 × 0.9 × 0.9 mm).

Image processing

Images were preprocessed using FSL (www.fmrib.ox.ac.uk) and AFNI (http://afni.nimh.nih.gov/afni) as implemented in the 1000 Functional Connectomes Project scripts (https://www.nitrc.org/projects/fcon_1000/). The first 5 EPI volumes were removed to allow for steady state tissue magnetization. EPI volumes were realigned to a mean image to correct for between-scan head movement, spatially normalized to the standard template of the Montreal Neurological Institute

(MNI), smoothed and detrended. Signal from white matter and CSF was regressed from voxel time series to remove non-neuronal BOLD fluctuations. We conducted our analysis both with and without GSR, where global signal is a calculated at each time point as the mean signal BOLD signal within a whole-brain mask. The set of 6 motion parameters from the realignment was also regressed out, and a mean motion summary measure retained for inclusion as a nuisance covariate in group level analysis (Van Dijk et al., 2012). Finally, the normalized volumes were temporally filtered (0.01–0.1 Hz).

Graph construction

The AAL template (Tzourio-Mazoyer et al., 2002) comprising 116 macro-anatomical regions, which is the most widely used atlas in the graph theory literature, was used to establish ROIs. The time series were extracted from each ROI by taking the mean signal in all voxels. FC was calculated as the pairwise correlation between all ROI time series, which resulted in a 116 × 116 connectivity matrix for each participant. Matrices were thresholded at connection densities of k = 5–25% (k, proportion of total connections retained). We analyzed both weighted and binary graphs. For the binary graphs, suprathreshold connections were then set to 1, resulting in graphs where 1 signified a connection and 0, no connection. Thresholding is important in binary graphs to exclude weak connections, which are assigned the same weight (1) as stronger connections. In weighted graphs, thresholding is still important as the sheer number of low weight connections can dominate the value of graph metrics, and graph metrics tend to those of random graphs as the connection density tends to 100%. Network features are known to vary with different numbers of links considered (Stam and Reijneveld, 2007; van Wijk et al., 2010), and so a range of connection densities (typically between 5–35%) is typically used. High thresholds (lower connection densities, i.e., 5–10%) correspond to networks comprising the strongest and presumably most important routes in a network, with functional units clearly separated into distinct modules, but higher connection densities also consider weaker links in the network, with greater cross-talk between modules.

Graph metrics

Non-normalized mean clustering coefficient (mC), global efficiency (Eg), modularity (Q), and rich-club coefficient (ϕ) were first calculated using the brain connectivity toolbox (Rubinov and Sporns, 2010). mC, Eg, and ϕ were then normalized to remove the effect of overall functional connectivity and basic network features such as degree distribution. Doing so more specifically elucidates the network structure, while removing contributions from lower level connectivity attributes. Normalization was achieved by dividing the values of mC, Eg, and ϕ by those obtained from a random network with the same number of nodes, links, and degree distribution (null networks). To obtain null networks, each link in the thresholded and binarized connectivity matrix was randomly reconnected an average of three times, and mC, Eg and ϕ calculated on the resulting random graph. This process was repeated 20 times, and the average of randomized mC, Eg, and ϕ calculated. γ, λ, and ϕ_{norm} are then defined as mC/mC_{rand}, Eg/Eg_{rand}, and ϕ/ϕ_{rand}, respectively. To calculate small-worldness (σ), γ and λ were multiplied, $\sigma = \gamma \times \lambda$, or equivalently $\sigma = \gamma \div \Lambda$, where Λ is the harmonic mean of path length.[1] Metrics were all normally distributed and did not require further transformation prior to genetic analysis. To reduce the influence of outliers, data were winsorized, with the maximum distance from the mean for all metrics set to three standard deviations. No more than 1.69% of the data were adjusted in this manner for any given graph metric.

[1] Path length between two nodes is the smallest number of links required to connect the two nodes.

Genetic modeling

MZ and DZ twin correlations were calculated for each metric via maximum likelihood estimation implemented in Mx (Neale et al., 2002). An MZ correlation higher than DZ correlation is indicative of a genetic contribution. We then used structural equation models (SEM) to estimate to what extent the variance in each metric was attributable to additive genetic, A, common environment, C, and unique environment/residual modeling error, E (Neale et al., 2002). Initially, variance models including all components A, C and E were fitted, including age, sex and mean head motion as covariates. This sample is a subset of that used in Couvy-Duchesne et al. (2014), which found that head-motion metrics are significantly heritable (35–57%), and highlights the importance of accounting for this source of heritability at the group level. We tested additive genetic models (ACE) rather than genetic dominance models (ADE), even though in some cases the MZ correlations were more than double the DZ correlations (Table 2a, b), since preliminary testing of ADE models (data not shown) indicated low power (i.e. wide confidence intervals) to discriminate A and D factors.

Parameters were successively dropped from the model, and reduced models were tested for goodness of fit. The model with greatest model parsimony as quantified by the lowest Akaike Information Criterion (AIC) was retained for heritability estimation.

In order to determine whether hub regions (those with high degree) were heritable, post hoc genetic modeling was applied to the degree of all 116 nodes. The degree of a node is simply the number of suprathreshold connections of that node, so no further calculations were required to obtain these metrics. Given the pattern of heritability observed for the global graph metrics, we chose a connection density of 10%, did not apply global signal regression, and used the weighted measure of degree.

Phenotypic relationships

Pairwise Pearson correlations between 3 of the graph metrics were calculated. σ was not included in either the correlational or multivariate genetic analysis, as it is a composite of two of the other metrics. Correlated metrics were tested in a multivariate ACE model using Cholesky decomposition (Neale et al., 2002) to see if the relationship could be attributed to common genetic factors, or common environmental factors influencing all phenotypes (Fig. 6).

Results

Network visualization

To visualize networks obtained over the range of connection densities, the mean over participants of each pairwise connection was taken, resulting in a groupwise graph, which was then thresholded (k = 5–35%) and binarized. This graph was decomposed into modules using the modularity algorithm of (Newman, 2006), and illustrated using BrainNet Viewer (http://www.nitrc.org/projects/bnv/; Xia et al., 2013; Fig. 1). Between k = 5 and 25% (Figs. 1a–c), a familiar pattern of resting state networks appears. The default mode network (DMN; blue), dorsal attention/task positive network (red), visual network (pink), subcortical (yellow), sensorimotor (cyan), cerebellar (green), and hippocampus/amygdala/temporal (black) are apparent at various connection densities. As the connection density is increased, different modules lose their distinction and merge, leading to fewer and larger modules. After k = 25%, the modular network architecture is lost. The main difference between global signal regression not implemented (a) and implemented (b), is that networks with GSR implemented are more modular, with more distinct modules observable.

Table 2
a and b: Mean (SD) of the five graph metrics (k = 5–25%) across the 592 participants Twin correlations, variance component estimates for A (additive genetic), C (common environment), and E (unique environment), and model fit for the five graph metrics, k = 5–25%. Computed without (Table 2a) and with (Table 2b) global signal regression.

Table 2a

Phenotype			Twin correlations (95% CI)		Model fit (AIC)[a]			Variance estimates (%) from best fitting model (95% CI)			
k		Mean (SD)	MZ (N = 84 pairs)	DZ (N = 89 pairs)	ACE	AE	CE	E	A	C	E
5	**ϒ**	3.14 (1.64)	0.45 (0.31, 0.58)	0.12 (−0.02, 0.25)	388.16	**386.16**	398.77	420.21	58 (42, 69)	–	42 (31, 58)
	Q	0.54 (0.08)	0.43 (0.28, 0.55)	0.23 (0.09, 0.36)	366.25	**365.82**	366.62	409.62	59 (45, 69)	–	41 (31, 55)
	φ_{norm}	1.02 (0.01)	0.21 (0.05, 0.37)	0.03 (−0.11, 0.17)	384.65	**382.65**	383.82	385.17	19 (1, 35)	–	81 (65, 99)
	λ	0.66 (0.08)	0.43 (0.28, 0.55)	0.15 (0.01, 0.29)	399.17	**397.17**	403.68	431.43	54 (40, 66)	–	46 (34, 60)
	σ	2.18 (1.28)	0.47 (0.32, 0.59)	0.11 (−0.03, 0.25)	387.81	**385.81**	399.38	420.52	58 (43, 70)	–	42 (30, 57)
10	**ϒ**	2.02 (0.80)	0.40 (0.25, 0.54)	0.13 (−0.01, 0.26)	386.18	**384.18**	390.68	412.63	51 (35, 63)	–	49 (37, 65)
	Q	0.40 (0.08)	0.36 (0.20, 0.50)	0.13 (–0.01, 0.27)	378.64	**376.79**	378.71	401.39	46 (31, 59)	–	54 (41, 69)
	φ_{norm}	1.02 (0.02)	0.29 (0.13, 0.44)	0.09 (−0.05, 0.23)	387.85	**385.85**	387.29	394.53	29 (12, 44)	–	71 (56, 88)
	λ	0.77 (0.07)	0.37 (0.21, 0.50)	0.16 (0.02, 0.30)	395.80	**393.82**	398.41	423.95	54 (39, 66)	–	46 (34, 61)
	σ	1.59 (0.71)	0.42 (0.28, 0.55)	0.13 (−0.01, 0.27)	384.32	**382.32**	390.46	414.06	54 (39, 66)	–	46 (34, 61)
15	**ϒ**	1.67 (0.52)	0.37 (0.21, 0.51)	0.14 (0.00, 0.28)	387.34	**385.37**	388.38	410.87	48 (32, 60)	–	52 (40, 68)
	Q	0.33 (0.08)	0.29 (0.13, 0.44)	0.13 (−0.01, 0.26)	379.95	**378.35**	378.67	395.24	40 (23, 54)	–	60 (46, 77)
	φ_{norm}	1.03 (0.02)	0.29 (0.12, 0.43)	0.08 (−0.06, 0.22)	380.32	**378.32**	380.33	387.67	29 (13, 44)	–	71 (56, 87)
	λ	0.82 (0.05)	0.35 (0.20, 0.49)	0.15 (0.02, 0.29)	395.92	**393.94**	397.78	420.68	52 (35, 64)	–	48 (36, 65)
	σ	1.39 (0.48)	0.39 (0.24, 0.52)	0.16 (0.02, 0.29)	383.53	**381.56**	385.44	411.11	51 (36, 63)	–	49 (37, 64)
20	**ϒ**	1.48 (0.37)	0.34 (0.18, 0.48)	0.15 (0.01, 0.28)	384.61	**382.96**	383.99	405.37	44 (28, 57)	–	56 (43, 72)
	Q	0.29 (0.07)	0.23 (0.07, 0.38)	0.13 (−0.01, 0.27)	382.67	382.06	**380.67**	392.77	–	29 (14, 42)	71 (58, 86)
	φ_{norm}	1.03 (0.03)	0.21 (0.05, 0.37)	0.10 (−0.04, 0.23)	366.51	**364.57**	364.96	370.25	24 (7, 39)	–	76 (61, 93)
	λ	0.86 (0.04)	0.31 (0.15, 0.46)	0.16 (0.02, 0.29)	395.77	**393.89**	395.91	414.61	45 (28, 59)	–	55 (41, 72)
	σ	1.28 (0.35)	0.36 (0.20, 0.49)	0.16 (0.02, 0.30)	380.51	**378.85**	380.45	405.02	48 (32, 60)	–	52 (40, 68)
25	**ϒ**	1.36 (0.28)	0.30 (0.14, 0.44)	0.14 (0.00, 0.28)	387.70	386.32	**386.19**	403.59	–	33 (19, 45)	67 (55, 81)
	Q	0.26 (0.07)	0.21 (0.05, 0.37)	0.11 (−0.03, 0.25)	390.68	389.54	**388.68**	397.72	–	26 (11, 39)	74 (61, 89)
	φ_{norm}	1.04 (0.03)	0.22 (0.05, 0.37)	0.15 (0.01, 0.28)	370.88	370.01	**368.88**	377.25	–	22 (9, 34)	78 (66, 91)
	λ	0.88 (0.04)	0.27 (0.11, 0.42)	0.18 (0.04, 0.31)	392.15	**390.63**	390.97	406.83	40 (23, 54)	–	60 (46, 77)
	σ	1.20 (0.27)	0.32 (0.16, 0.46)	0.17 (0.03, 0.30)	382.35	**381.10**	381.14	402.53	44 (28, 57)	–	56 (43, 72)

Table 2b

Phenotype		Twin correlations (95% CI)			Model fit (AIC)				Variance estimates (%) from best fitting model (95% CI)		
k		Mean (SD)	MZ (N = 84 pairs)	DZ (N = 89 pairs)	ACE	AE	CE	E	A	C	E
5	**ϒ**	6.46 (1.44)	0.19 (0.03, 0.35)	0.17 (0.03, 0.30)	410.62	409.12	**408.78**	416.62	–	22 (8, 35)	78 (65, 92)
	Q	0.68 (0.04)	0.17 (0.01, 0.33)	0.17 (0.03, 0.30)	399.07	398.49	**397.07**	405.38	–	24 (9, 37)	76 (63, 91)
	φ_{norm}	1.07 (0.03)	0.07 (–0.09, 0.24)	−0.03 (−0.17, 0.11)	445.81	443.81	444.02	**442.06**	–	–	100 (100, 100)
	λ	0.63 (0.06)	0.32 (0.16, 0.46)	0.01 (−0.13, 0.15)	420.86	**418.86**	423.07	426.44	30 (11, 46)	–	70 (54, 89)
	σ	4.14 (1.11)	0.19 (0.03, 0.35)	0.11 (−0.03, 0.25)	425.64	**423.64**	424.41	428.36	24 (6, 40)	–	76 (60, 94)
10	**ϒ**	4.06 (0.55)	0.19 (0.02, 0.34)	0.12 (−0.02, 0.26)	400.51	398.77	**398.74**	404.73	–	21 (7, 34)	79 (66, 93)
	Q	0.57 (0.04)	0.22 (0.05, 0.37)	0.04 (−0.10, 0.17)	419.05	**417.05**	419.68	421.61	28 (7, 46)	–	72 (54, 93)
	φ_{norm}	1.10 (0.04)	−0.01 (−0.17, 0.16)	−0.04 (−0.18, 0.10)	432.73	430.73	430.73	**428.73**	–	–	100 (100, 100)
	λ	0.75 (0.04)	0.26 (0.09, 0.41)	–0.01 (–0.15, 0.13)	426.71	**424.71**	427.35	428.94	23 (5, 40)	–	77 (60, 95)
	σ	3.06 (0.47)	0.20 (0.03, 0.36)	0.12 (−0.02, 0.26)	407.75	**405.98**	405.99	412.11	27 (9, 42)	–	73 (58, 91)
15	**ϒ**	3.09 (0.28)	0.10 (–0.07, 0.26)	0.04 (−0.10, 0.18)	397.58	**395.60**	395.69	395.65	13 (0, 30)	–	87 (70, 100)
	Q	0.51 (0.03)	0.20 (0.04, 0.36)	0.01 (−0.13, 0.15)	421.95	**419.95**	422.24	422.70	24 (2, 43)	–	76 (57, 98)
	φ_{norm}	1.13 (0.05)	0.08 (−0.09, 0.24)	0.14 (0.00, 0.28)	435.06	434.25	**433.06**	435.54	–	16 (1, 29)	84 (71, 99)
	λ	0.79 (0.03)	0.31 (0.15, 0.45)	−0.03 (−0.16, 0.11)	414.39	**412.39**	416.43	419.19	28 (10, 44)	–	72 (56, 90)
	σ	2.43 (0.24)	0.12 (−0.05, 0.28)	0.05 (−0.09, 0.19)	396.23	**394.25**	394.35	395.03	15 (0, 31)	–	85 (69, 100)
20	**ϒ**	2.56 (0.17)	0.09 (−0.08, 0.25)	−0.02 (−0.16, 0.12)	390.79	388.79	389.20	**387.48**	—	—	100 (100, 100)
	Q	0.46 (0.03)	0.19 (0.02, 0.35)	0.00 (−0.14, 0.14)	421.04	**419.04**	420.88	420.77	21 (0, 39)	–	79 (61, 100)
	φ_{norm}	1.16 (0.07)	0.02 (−0.15, 0.19)	0.05 (−0.09, 0.19)	433.36	431.57	431.36	**429.94**	–	–	100 (100, 100)
	λ	0.79 (0.02)	0.30 (0.14, 0.44)	−0.00 (−0.14, 0.14)	421.06	**419.06**	422.63	425.97	28 (10, 44)	–	72 (56, 90)
	σ	2.03 (0.13)	0.05 (−0.11, 0.22)	0.01 (−0.13, 0.15)	370.28	368.28	368.35	**366.76**	–	–	100 (100, 100)
25	**ϒ**	2.21 (0.13)	0.11 (−0.06, 0.27)	−0.07 (−0.20, 0.07)	404.25	402.25	402.81	**400.87**	–	–	100 (100, 100)
	Q	0.42 (0.03)	0.14 (−0.03, 0.30)	0.00 (−0.14, 0.14)	415.69	413.69	414.53	**413.45**	–	–	100 (100, 100)
	φ_{norm}	1.18 (0.08)	0.06 (−0.11, 0.22)	−0.01 (−0.15, 0.13)	454.45	452.45	452.56	**450.64**	–	–	100 (100, 100)
	λ	0.80 (0.02)	0.31 (0.15, 0.46)	−0.00 (−0.14, 0.14)	421.25	**419.25**	423.53	427.16	30 (12, 47)	–	70 (53, 88)
	σ	1.76 (0.08)	0.01 (−0.15, 0.18)	−0.05 (−0.19, 0.09)	369.29	367.29	367.29	**365.29**	–	–	100 (100, 100)

Best model indicated in bold font.
[a] Where an AE model has only a slightly worse fit than a CE model, and vice versa, both models are worthy of consideration. In addition, confidence intervals for ACE estimates were wide indicating low power to discriminate between A and C.

Graph theory metric means

The means of our five metrics are given in Table 2a and b. The mean values of the metrics are typical of those seen in the literature (e.g. Achard et al., 2006; Lord et al., 2012), and indicate small-world, modular, rich-club topology, irrespective of methodological choices. However, the means of the metrics do differ depending on methodological choices, indicating that the nature of the networks obtained varies. The choice of threshold has a strong effect on the metric means and variances, with γ, λ, and σ tending to 1 as k increases, indicating a loss of small-world properties as the addition of weaker connections causes a shift toward random graphs. Likewise, Q reduces as k increases, indicating a loss of modular architecture, as depicted in Fig. 1. We thus henceforth primarily discuss results at k = 10%, which we believe to represent an optimal balance between removing spurious weak connections on the one hand and avoiding graph fragmentation on the other (observed to occur extensively at a threshold of 5%). The behavior of ϕ_{norm} with k was less straightforward and depended on GSR and

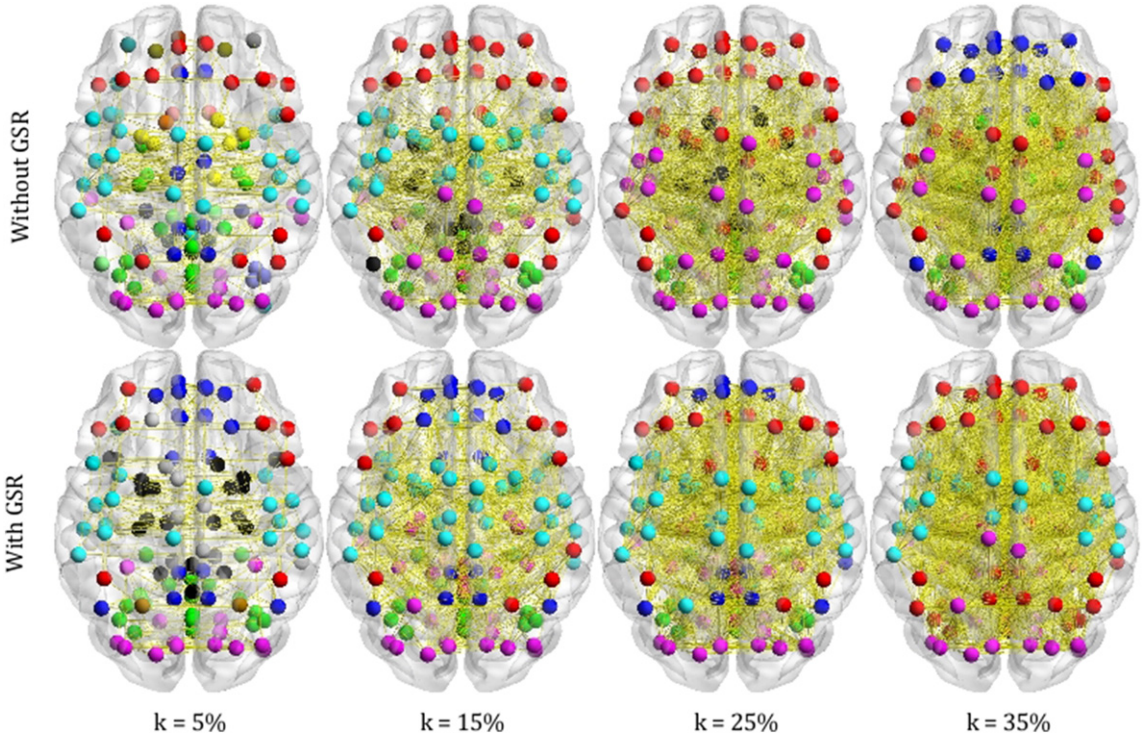

Fig. 1. Modular decomposition of groupwise mean network over a range of connection densities (i.e. k = 5–35%), without and with global signal regression (GSR). Yellow lines indicate a suprathreshold connection and node colors indicate module membership (DMN (blue), dorsal attention network (red), visual network (pink), subcortical (yellow), sensorimotor (cyan), hippocampus/amygdala/temporal (black). As the connection density increases, different modules lose their distinction and merge, leading to fewer and larger modules. After k = 25%, the modular network architecture is lost.

binarizing (Table 2a,b and Supplementary Table 1a,b). γ, Q, ϕ_{norm} and σ are greatly increased if GSR is employed (mean % change = 143%, 50%, 7%, 150%, respectively, at k = 10%, paired t-test $p < 10^{-15}$), while λ is relatively unchanged (−1% at k = 10%, $p < 10^{-4}$). Finally, binarizing seems to have little effect on numeric values of γ, Q, λ, σ (−1%, −6%, 2%, 1%, respectively, at k = 10% $p < 10^{-15}$), but a large effect on ϕ_{norm} (40% at k = 10% $p < 10^{-15}$).

Heritability

Heritability estimates were seen to vary substantially depending on threshold and implementation of global signal regression and were weakly affected by binarizing. Generally, heritability estimates were higher at lower connection densities, without global signal regression and without binarizing. Without GSR, all metrics had a higher MZ

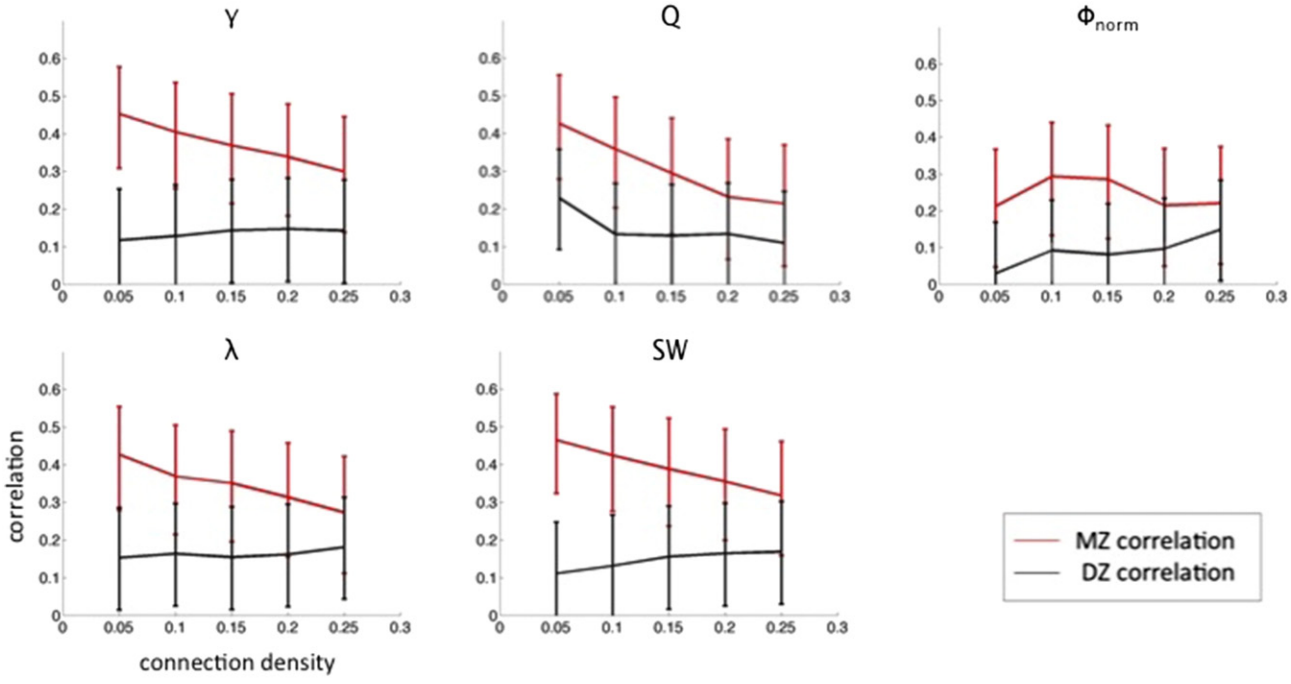

Fig. 2. Monozygotic (MZ), dizygotic (DZ) twin correlations across metrics and thresholds, GSR not implemented; error bars represent 95% confidence intervals.

correlation than DZ correlation over the whole range of connection densities (Fig. 2), both for weighted (Table 2a) and binary graphs (Supplementary Table 1a), indicating a genetic contribution. MZ correlations ranged from 0.22 to 0.42 across metrics and connection densities and were significant at all k, whereas DZ correlations ranged from 0.10 to 0.20 and were not all significant (95% confidence intervals crossed zero). SEM revealed that all metrics had significant estimates of genetic variance (a^2) over a certain range of connection densities (Table 2a, Fig. 3). Dropping the C parameter gave improved model parsimony for all metrics over connection densities 5–15%. At k = 20% and above, the best fitting model was CE for some metrics. However, notably, the fit of the AE and CE models were often very similar. The heritability estimates (i.e., A ($=a^2$)) for the best fitting model are given in Table 2a. γ, Q, λ, and σ were all strongly heritable, (51, 46, 54, 54%, respectively, k = 10%) with similar estimates for binary networks. ϕ_{norm} was moderately heritable (29%, k = 10%) for weighted graphs, but not for binary networks. As k increased from 10–25%, progressively more variance is attributed to unique environmental variance and/or modeling/experimental error for all metrics.

The heritability estimates varied little between weighted and binary graphs with the exception of ϕ_{norm} which for binary networks has best fitting model without genetic component. The heritability of Q was lower for binary compared to weighted graphs at k = 5–10%, and at k = 15% and above the best fitting model did not have a genetic component.

Regressing out global signal substantially reduced the heritability estimates (Table 2b, Fig. 4). At k = 10%, Q, λ, and σ were moderately heritable (28%, 23% and, 27%), whereas γ and ϕ_{norm} had a best fitting model without a genetic component, although AE and CE models had similar fit. As with the no global signal regression case, binarizing had little effect on heritability estimates (Supplementary Table 2), although γ_{binary} had a best fitting model with genetic component and corresponding a^2 of 26 (8, 42), and Q had best fitting model without genetic component, and as k increased beyond 10%, variance attributable to unique environmental/modeling error increased (See Supplementary Table 1a–b).

The spatial distribution of genetic influences on degree, at a connection density of 10%, without global signal regression, is summarized in Supplementary Table 3 and Fig. 5. Genetic influences varied across the brain and do not appear to cluster specifically to any of the functional modules depicted in Fig. 1. 47 out of 116 regions were significantly heritable, and these regions were distributed approximately evenly across the brain, with a slight over-representation in the occipital lobe (9/14 regions), and under-representation in parietal lobes (4/12 regions) and subcortex (2/10 regions). Of the 47 regions, 18 were bilateral pairs, 10 were left lateralized, 15 were right lateralized, and 4 were in the vermis. There was no correlation between the degree of a node and its heritability derived from the best fitting model (r = 0.12, p = 0.21), and the high degree hubs were no more heritable than the other nodes. When heritability is extracted from the full ACE model, there is a weak correlation (r = 0.19, p = 0.04) between heritability and degree. Further, a large proportion of nodes (66/116) had best fitting models without additive genetic variance, of which 50/116 had a significant common environmental variance (See Table S3).

In addition, we found strong phenotypic correlations among the different network measures (Table 3). Without GSR, all metrics were significantly correlated with the others, with the highest correlation at k = 10% being 0.92 between γ and Q. With GSR implemented, the correlations were generally lower (highest was 0.63 between γ and Q), suggesting that global signal fluctuations represent a common source of variance for the different metrics. With GSR, Q and λ were negatively correlated, reflecting the trade-off between separation of and integration between modules. A similar pattern of correlations was seen across k both with and without GSR (Supplementary Table 2a–d). The one exception to this is with GSR at k > 20%, where the correlation between λ and γ also becomes negative.

A multivariate genetic analysis was used to estimate the shared genetic contribution across metrics. Without GSR, a single genetic factor, A1, accounted for most of the genetic variance in all of the metrics at all connection densities ($A1/A_{total}$ = 93%, 87% for Q and λ, respectively, at k = 10%). With GSR implemented, 40% of the genetic variance (12% of the total variance) in Q was accounted for by a second genetic factor A2, which also accounted for 97% of the genetic variance in λ (Fig. 6). The path coefficients for the second genetic factor were the opposite sign for Q and λ, meaning that if this factor increases modularity, then the same factor will reduce λ. At higher connection densities, the

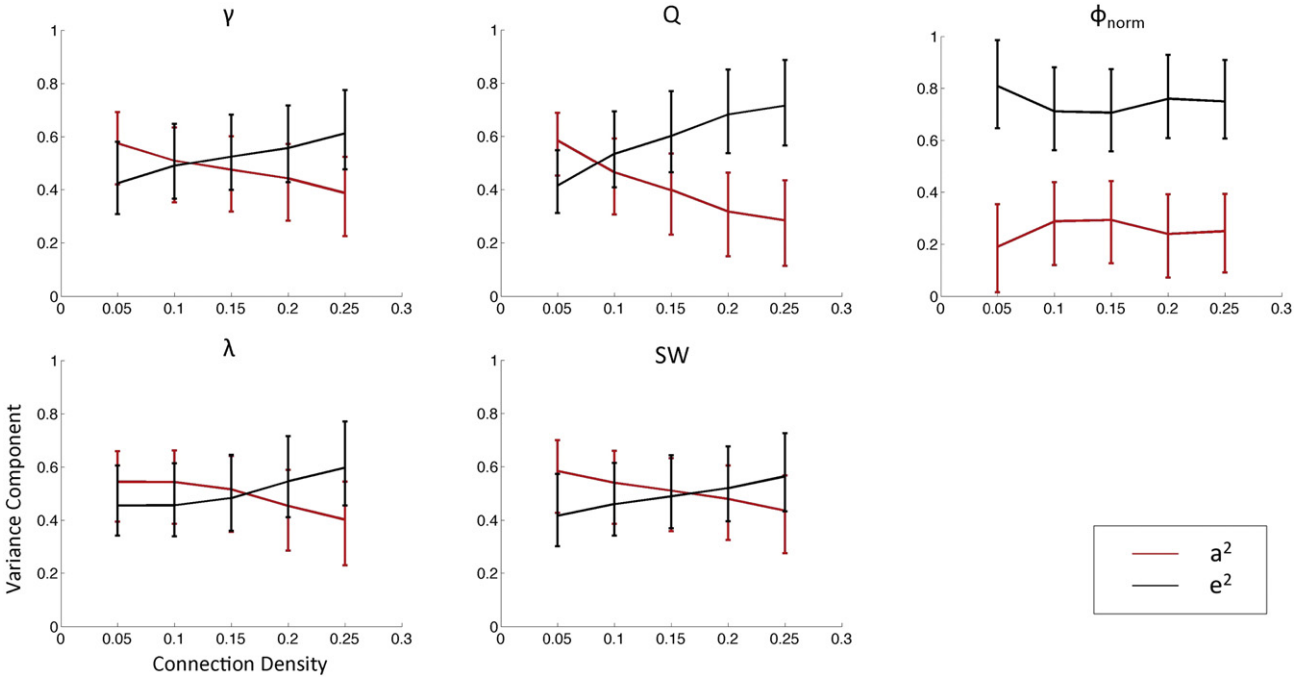

Fig. 3. Additive genetic (a^2) and unique environmental (e^2) variance components across metrics and thresholds, GSR not implemented.

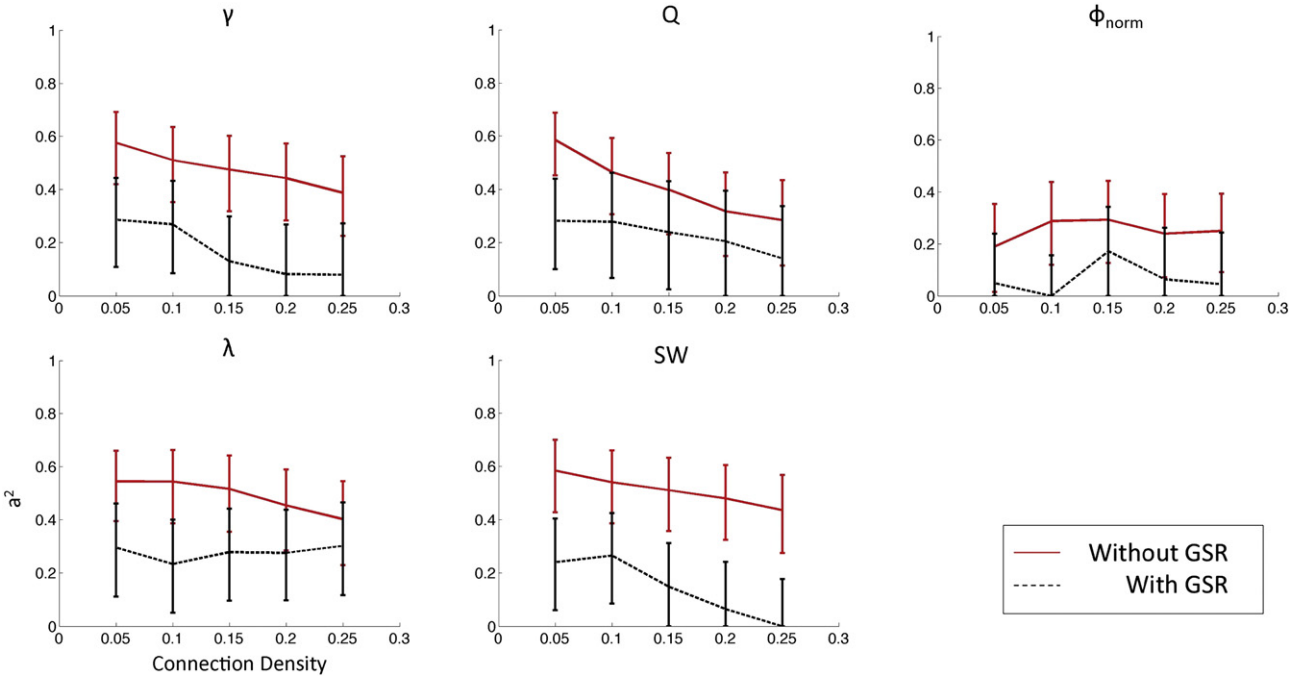

Fig. 4. Additive genetic variance components across metrics and thresholds estimated both without (solid line) and with (dashed line) global signal regression (GSR). Heritability estimates are much reduced with GSR implemented.

independent genetic factors (A2, A3) were reduced (Supplementary Table 2a–d) and not significant, and most of variance was attributed to a single genetic factor, A1. This is related to the increasing correlations between the metrics at higher connection densities.

Multivariate models also revealed overlapping environmental influences/experimental error on the different metrics. Without GSR, The environmental influences on γ and Q overlapped, with sources influencing environmental variance in γ accounting for 75% ($E1/E_{total}$) of the environmental variance in Q. This same factor accounted for only 23% of the environmental variance in λ. A second environmental factor accounted for 23% of the environmental variance in Q, and 3% of the environmental variance in λ, and a final unique environmental factor accounted for the remaining 75% of the environmental variance in λ. With GSR implemented, the overlapping environmental/error influences were much reduced, with the majority of environmental variance in Q and λ attributed to E2 and E3, respectively, implying that without GSR implemented, much of E1 is due to global signal.

Discussion

This study shows that network characteristics of resting state functional activity are partially under genetic influence and that heritability estimates vary substantially depending on methodological choices. We found that γ (h^2 = 47–61%), Q (h^2 = 38–59%), λ (h^2 = 52–64%), and σ (h^2 = 51–59%) were strongly influenced by genetic factors at connection densities ranging between k = 5–15%, with heritability reducing at k > 15%. Heritability estimates were substantially lower when global signal regression was implemented h^2 (γ = 0–26%, Q = 0–28%, ϕ_{norm} = 0%, λ = 23–30%, σ = 0–27%) and there was little difference between considering weighted graphs or binary graphs, other than for ϕ_{norm}. Furthermore, these heritable traits were moderately correlated (|r| = 0.62–0.92, without GSR, 0.27–0.63 with GSR) and largely influenced by overlapping genetic factors.

The heritability of global efficiency is largely consistent with prior studies of rs-fMRI graph metrics. Fornito et al. (2011) found a heritability of 60 (CI:17, 83)% (without GSR) for cost efficiency in 58 adults (cost efficiency reflects the trade-off between the need for efficiency in a network and the cost of wiring). In 86 young children (mean age 12), van den Heuvel et al. (2013) estimated a heritability of 42 (CI:5, 73)% for λ, but no genetic influence on γ (without GSR). While the results for λ are similar, the participants were younger, and genetic and environmental effects on a trait can change with age (e.g. Bartels et al., 2002; Lenroot et al., 2009). Furthermore, their analysis was performed using voxel-wise networks, where each voxel constitutes a network node. Such networks differ topologically from anatomically informed networks, and they are "scale-free" (van den Heuvel et al., 2008)—i.e., dominated by very highly connected hubs (Barabasi and Albert, 1999). In contrast to the previous two studies, we detect significant heritability of γ. This may represent methodological differences (van den Heuvel et al. (2013) did not correct for white matter signal, csf signal, or motion

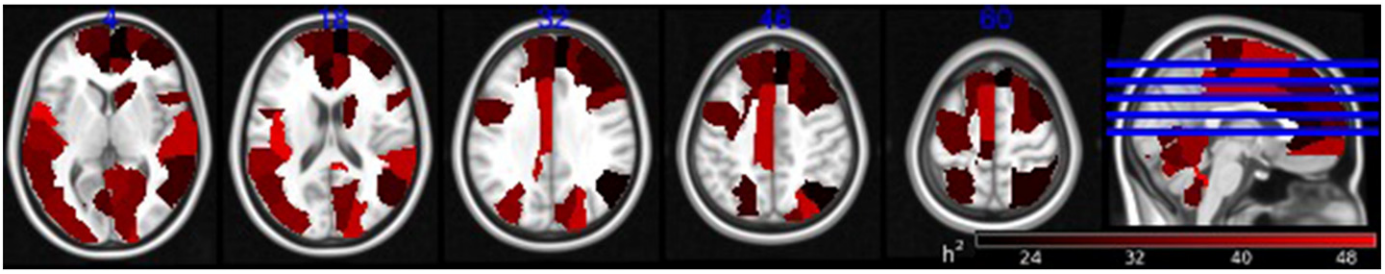

Fig. 5. Regions with significant heritability for weighted degree at connection density of 10%, without global signal regression.

Table 3
Multivariate genetic analyses of mean clustering (γ), modularity (Q), and global efficiency (λ) at k = 10%.

k = 10%	Phenotypic correlation (Pearson's)		h^2	Breakdown of total variance (as Cholesky decomposition), shown as a % with 95% confidence intervals					
				Additive genetic sources			Unshared environmental sources		
	ϒ	Q		A1	A2[a]	A3	E1	E2	E3
Without GSR									
ϒ	1.00		52	52 (37, 64)			48 (36, 63)		
Q	0.92 (0.91, 0.93)	1.00	49	45 (31, 57)	3 (0, 6)		38 (27, 52)	12 (9, 16)	
λ	0.72 (0.67, 0.76)	0.62 (0.56, 0.67)	55	49 (33, 66)	0 (0, 3)	7 (0, 6)	10 (4, 21)	1 (0, 5)	34 (26, 44)
With GSR									
ϒ	1.00		27	27 (9, 43)			73 (57, 91)		
Q	0.64 (0.59, 0.69)	1.00	29	18 (2, 39)	12 (1, 24)		25 (13, 42)	47 (35, 60)	
λ	0.26 (0.19, 0.34)	−0.36 (−0.43, −0.29)	25	1 (0, 12)	24 (5, 43)	0 (0, 9)	7 (1, 18)	27 (15, 44)	41 (33, 49)

[a] Factor A2 has opposing effects (+ve for Q, but –ve for λ).

confounds), but may also reflect that the previous two studies were underpowered, emphasizing the necessity of large sample sizes for heritability estimates. We performed power calculations (Neale and Cardon, 1992) based on the effect sizes in our sample and determined that the sample sizes (number of twin pairs) required to reject the null hypothesis of no genetic component at a significance level of 0.05, with a power of 50% were (203, 97, 482, 5531 for λ(no GSR), γ(no GSR), λ(GSR), γ(GSR) respectively, k = 10%), indicating that our study was underpowered for detecting heritability with GSR implemented, but sufficiently powered without GSR implemented.

Our heritability estimates are similar to those for other functional-imaging derived measures such as activation in N-Back working memory tasks, (h^2 ~ 0–65%) (Blokland et al., 2011), and connectivity in the default mode network $h^2 = 42 \pm 17\%$ (Glahn et al., 2010). They are lower than for cognitive phenotypes such as intelligence (h^2 ~ 50–80%) (Plomin and Spinath, 2004) and performance on working memory tasks (h^2 ~ 40–60%) (e.g., Ando et al., 2001; Polderman et al., 2006).

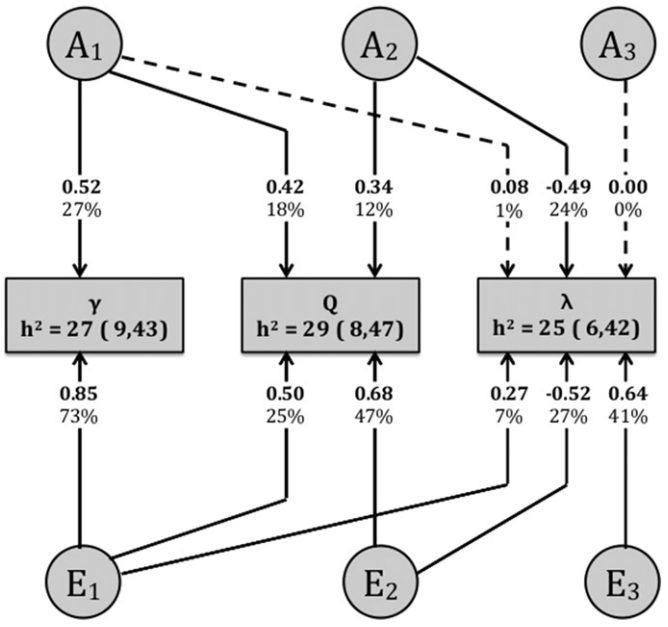

Fig. 6. Path diagram for multivariate genetic model showing genetic and environmental sources of covariation between three metrics, with parameter estimates given for k = 10%, GSR implemented. Path labels give standardized path coefficients (bold) and variance components (the square of the path coefficients) of each factor. Thus, the genetic factor influencing γ also accounts for 18% of the total variation in Q (60% of the genetic variation), and 1% of the variation in λ. Q has a second genetic factor accounting for 12% of its variation, which also accounts for 24% of the variation in λ. Whereas overlapping genetic factors accounted for much of genetic variation in the metrics, separate environmental factors account for the majority of environmental variance in Q (47%) and λ (41%). Heritability (the sum of sources of genetic variance for each variable; h^2) is shown for each variable. Non-significant path coefficients are shown by dotted arrows.

γ, λ, and σ may be collectively described as the small-world properties of networks. Small-world networks allow strong contact between groups of nodes with common functionality and simultaneously allow highly efficient information transfer via a small number of long-range connections (Watts and Strogatz, 1998). Many studies (e.g. Salvador et al., 2005; Achard et al., 2006) have reported that the small-world architecture applies to human brain functional networks, and we observe the same in this data set (mean (SD) γ = 2.02 (0.80), mean λ = 0.77 (0.07), k = 10%, Table 2). This study demonstrates that this favorable set-up is substantially conferred by genetic factors. Furthermore, as we increase the connection density of the networks, and the small-world properties of the graph reduce (γ decreases, λ increases), we see a corresponding drop-off in heritability, suggesting an underlying genetic influence which is only observed when the chosen connection density appropriately balances removal of weak and confounding connections with avoidance of network fragmentation. We believe this balance is best achieved at lower thresholds at around k = 10%, as this is where we observe highest penetrance of genetic effects, and highest small-world properties.

In addition to high clustering and high efficiency, brain networks are modular (Beckmann et al., 2005; He et al., 2009): the nodes separate into modules with many strong connections between nodes within the same module, and relatively few between modules. Modularity measures this separation into distinct sub-networks with particular functions such as the visual, sensorimotor, and default mode networks, etc. Here we find a genetic contribution to modularity of (h^2 = 0–59%), a result not previously observed in other studies of the heritability of functional connectivity.

Recently, brain functional networks have been observed to display a "rich-club" organization, whereby the network hubs (nodes with the largest number of connections) are highly connected to each other, forming a network core (van den Heuvel and Sporns, 2011); most of the shortest paths between nodes in the network pass via this rich club. Such organization is hypothesized to give the network higher resilience against targeted attack of hubs (Kaiser et al., 2007; van den Heuvel and Sporns, 2011). Here, we did not find strong evidence that the rich-club coefficient is heritable. ϕ_{norm} showed the most variability between the binary and weighted analysis, did not show the tendency to randomness as connection density increased as did the other metrics, and yielded the lowest heritability parameters. Thus, ϕ_{norm} appears to be the least promising phenotype for use as a genetic biomarker' however, it is important to note that in the context of brain imaging, ϕ_{norm} was originally defined on structural data (van den Heuvel and Sporns, 2011), not resting state functional data. In addition to the low heritability of rich club, our results do not support the idea of highly heritable hub regions. Only 47 of 116 nodes had a significant additive genetic variance component for degree, and there was no correlation between the degree of a node and its heritability, meaning that the degree of hubs is

no more heritable than that of other nodes. This is at odds with the idea of a genetically mediated network core of functional connectivity (c.f. Fornito et al., 2011).

The network metrics were correlated (Table 3), suggesting that common genetic or environmental factors might produce an advantageous network structure. Without GSR, the genetic source influencing γ also accounts for a common set of genes that were responsible for 93% and 87% of the genetic variance in Q and λ, respectively. This may represent a single set of genetic processes giving rise to distinct network characteristics, or it may represent a common underlying factor to all metrics, unrelated to network architecture, which has not been accounted for, such as the global signal. With GSR implemented, genetic influences were partitioned into two main factors, with one influencing γ and Q, and the second influencing Q and λ. γ and Q both measure features of network segregation and would be expected to be highly correlated and share common genetic underpinnings. More interestingly, Q and λ were significantly negatively correlated and almost all of the genetic variation in λ was accounted for by the second genetic factor influencing Q. Further, the set of genes which contributed positively to Q, negatively influence λ, indicating that this set of genes may regulate to trade-off between the separation of and the integration between modules. The phenotypic correlations between metrics were also mediated in part by environmental factors. γ and Q and λ were all influenced to varying degrees by overlapping environmental factors or correlated measurement error, so all phenotypic correlations between metrics have both genetic and environmental origins.

An important implication of this study is that the heritability of graph metrics is substantially reduced with global signal regressed out. The origin of the global signal is uncertain, but it may have non-neuronal (cardiac, respiratory) as well as neuronal (e.g. ascending arousal systems) contributions (Fox et al., 2009). Global signal fluctuations are considered by many as a nuisance confound giving rise to artificial correlations between unrelated time series. There is ongoing debate as to the nature of anti-correlations introduced by global signal regression (Murphy et al., 2009; Fox et al., 2009). For this reason, we have carried out the analysis both with and without GSR. The results of this paper imply that a large proportion of the heritability estimates are dependent on these global signal fluctuations, and further, that global signal represents a common cause of variance in the different metrics, with all metrics strongly correlated and sharing a largely identical set of genetic influences when global signal is not accounted for. The two papers reporting heritability of network efficiency (Fornito et al., 2011; van den Heuvel et al., 2013) did not account for global signal and reported similar estimates to those in this study without global signal accounted for. It is not clear which feature of the global signal contributes to the enhanced heritability estimates for the graph metrics. Since global signal regression is designed to remove physiological, non-neuronal contributions to the BOLD signal, itself a complex combination of neuronal, vascular, and metabolic factors (Liu, 2013); this raises the possibility that the high heritability of graph metrics seen here, and in previous studies (Fornito et al., 2011; van den Heuvel et al., 2013), may primarily represent the graph characteristics of vascular, as opposed to neural networks.

The current study has some limitations. The sample size is modest for establishing the importance of genetics and environment for phenotype as indicated by relatively wide confidence intervals, particularly for DZ twins where the confidence intervals spanned zero. Our multivariate analysis may suggest one set of genes regulating the trade-off between network modularity and network efficiency, with another set of genes influencing γ, but this finding is not robust to choice of threshold or binarizing. Secondly, the difference in heritability estimates when global signal regression is implemented may indicate that a proportion of the heritability is related to non-neuronal fluctuations in the BOLD signal, since GSR aims to remove such fluctuations. Indeed, γ and Q increase when global signal regression is implemented (λ_{binary} increases, $\lambda_{weighted}$ reduces), perhaps reflecting that the resulting graphs better "capture" the underlying favorable network properties. Some non-neuronal influences can be ruled out as contributing to the heritability estimates. Head motion was corrected for both at the subject level by regressing 6 head-motion parameters from voxel time series, and at the group level by inclusion of a mean-motion covariate. Overall levels of functional connectivity (and their neuronal and non-neuronal origins) are implicitly controlled for by normalizing metrics to those of random graphs with the same overall level of functional connectivity (and other low level network characteristics such as degree distribution). Another limitation of this study is the relatively short scan time of 5 min 15 s. Though scan times of 5–7 min are typical in resting state experiments, Birn et al. (2013) demonstrate that the test–retest reliability of functional connectivity estimates increase with scan time, plateauing at 8–12 min. The short scan time may contribute to the under-power of some of our statistical tests.

Despite these limitations, to date, this is the largest study of twins with fMRI resting state scans, allowing the strongest and most comprehensive current estimates of network heritability. We find the first evidence of heritability of γ and Q, and strong evidence that λ is heritable. We used a range of the most common and consensual processing procedures for both resting state fMRI and graph theory, to make these results as applicable as possible to prior studies using these metrics.

Acknowledgments

We thank the twins and siblings for their participation, Marlene Grace and Ann Eldridge for twin recruitment, Aiman Al Najjar and other radiographers for scanning, Kerrie McAloney and Daniel Park for research support, and staff in the Molecular Epidemiology Laboratory for DNA sample processing and preparation. This study was supported by the National Institute of Child Health and Human Development (R01 HD050735), and the National Health and Medical Research Council (NHMRC 486682, 1009064), Australia. Genotyping was supported by the NHMRC (grant 389875). BS is supported by ANZ Trustees PhD Scholarship in Medical Research. GZ is supported by an ARC Future Fellowship (FT0991634).

Appendix A. Supplementary data

Supplementary data to this article can be found online at http://dx.doi.org/10.1016/j.neuroimage.2015.07.048.

References

Achard, S., Salvador, R., Whitcher, B., Suckling, J., & Bullmore, E., 2006. A resilient, low-frequency, small-world human brain functional network with highly connected association cortical hubs. J. Neurosci. 26, 63–72.

Ando, J., Ono, Y., & Wright, M.J., 2001. Genetic structure of spatial and verbal working memory. Behav. Genet. 31, 615–624.

Barabasi, A.L., & Albert, R., 1999. Emergence of scaling in random networks. Science 286, 509–512.

Bartels, M., Rietveld, M.J., Van Baal, G.C., & Boomsma, D.I., 2002. Genetic and environmental influences on the development of intelligence. Behav. Genet. 32, 237–249.

Beckmann, C.F., DeLuca, M., Devlin, J.T., & Smith, S.M., 2005. Investigations into resting-state connectivity using independent component analysis. Philos. Trans. R. Soc. Lond. B Biol. Sci. 360, 1001–1013.

Birn, R.M., Molloy, E.K., Patriat, R., Parker, T., Meier, T.B., Kirk, G.R., Nair, V.A., Meyerand, M.E., & Prabhakaran, V., 2013. The effect of scan length on the reliability of resting-state fMRI connectivity estimates. NeuroImage 83, 550–558.

Blokland, G.A., McMahon, K.L., Thompson, P.M., Martin, N.G., de Zubicaray, G.I., & Wright, M.J., 2011. Heritability of working memory brain activation. J. Neurosci. 31, 10882–10890.

Couvy-Duchesne, B., Blokland, G.A.M., Hickie, I.B., Thompson, P.M., Martin, N.G., de Zubicaray, G.I., McMahon, K.L., & Wright, M.J., 2014. Heritability of head motion during resting state functional MRI in 462 healthy twins. NeuroImage 102, 424–434.

Damoiseaux, J.S., & Greicius, M.D., 2009. Greater than the sum of its parts: a review of studies combining structural connectivity and resting-state functional connectivity. Brain Struct. Funct. 213, 525–533.

de Zubicaray, G.I., Chiang, M.C., McMahon, K.L., Shattuck, D.W., Toga, A.W., Martin, N.G., Wright, M.J., & Thompson, P.M., 2008. Meeting the challenges of neuroimaging genetics. Brain Imaging Behav. 2, 258–263.

Dennis, E.L., Jahanshad, N., Toga, A., Brown, J., Rudie, J., Bookheimer, S., Dapretto, M., Johnson, K., McMahon, K., & de Zubicaray, G., 2011. Heritability of structural brain connectivity network measures in 188 twins. SFN 2011, Washington, D.C.

Fornito, A., Zalesky, A., Bassett, D.S., Meunier, D., Ellison-Wright, I., Yucel, M., Wood, S.J., Shaw, K., O'Connor, J., Nertney, D., Mowry, B.J., Pantelis, C., & Bullmore, E.T., 2011. Genetic influences on cost-efficient organization of human cortical functional networks. J. Neurosci. 31, 3261–3270.

Fox, M.D., & Raichle, M.E., 2007. Spontaneous fluctuations in brain activity observed with functional magnetic resonance imaging. Nat. Rev. Neurosci. 8, 700–711.

Fox, M.D., Zhang, D., Snyder, A.Z., & Raichle, M.E., 2009. The global signal and observed anticorrelated resting state brain networks. J. Neurophysiol. 101, 3270–3283.

Glahn, D.C., Winkler, A.M., Kochunov, P., Almasy, L., Duggirala, R., Carless, M.A., Curran, J.C., Olvera, R.L., Laird, A.R., Smith, S.M., Beckmann, C.F., Fox, P.T., & Blangero, J., 2010. Genetic control over the resting brain. Proc. Natl. Acad. Sci. U. S. A. 107, 1223–1228.

He, Y., Wang, J., Wang, L., Chen, Z.J., Yan, C., Yang, H., Tang, H., Zhu, C., Gong, Q., Zang, Y., & Evans, A.C., 2009. Uncovering intrinsic modular organization of spontaneous brain activity in humans. PLoS One 4, e5226.

Honey, C.J., Sporns, O., Cammoun, L., Gigandet, X., Thiran, J.P., Meuli, R., & Hagmann, P., 2009. Predicting human resting-state functional connectivity from structural connectivity. Proc. Natl. Acad. Sci. U. S. A. 106, 2035–2040.

Kaiser, M., Martin, R., Andras, P., & Young, M.P., 2007. Simulation of robustness against lesions of cortical networks. Eur. J. Neurosci. 25, 3185–3192.

Lebel, C., Walker, L., Leemans, A., Phillips, L., & Beaulieu, C., 2008. Microstructural maturation of the human brain from childhood to adulthood. NeuroImage 40, 1044–1055.

Lenroot, R.K., Schmitt, J.E., Ordaz, S.J., Wallace, G.L., Neale, M.C., Lerch, J.P., Kendler, K.S., Evans, A.C., & Giedd, J.N., 2009. Differences in genetic and environmental influences on the human cerebral cortex associated with development during childhood and adolescence. Hum. Brain Mapp. 30, 163–174.

Li, Y., Liu, Y., Li, J., Qin, W., Li, K., Yu, C., & Jiang, T., 2009. Brain anatomical network and intelligence. PLoS Comput. Biol. 5, e1000395.

Liu, T.T., 2013. Neurovascular factors in resting-state functional MRI. NeuroImage 80, 339–348.

Lord, A., Horn, D., Breakspear, M., & Walter, M., 2012. Changes in community structure of resting state functional connectivity in unipolar depression. PLoS One 7, e41282.

Maslov, S., & Sneppen, K., 2002. Specificity and stability in topology of protein networks. Science 296, 910–913.

Murphy, K., Birn, R.M., Handwerker, D.A., Jones, T.B., & Bandettini, P.A., 2009. The impact of global signal regression on resting state correlations: are anti-correlated networks introduced? NeuroImage 44, 893–905.

Neale, M., & Cardon, L., 1992. Methodology for genetic studies of twins and families. Springer.

Neale, M., Baker, S., Xie, G., & Maes, H., 2002. Mx: Statistical modeling. 6th ed.

Newman, M.E., 2006. Modularity and community structure in networks. Proc. Natl. Acad. Sci. U. S. A. 103, 8577–8582.

Plomin, R., & Spinath, F.M., 2004. Intelligence: genetics, genes, and genomics. J. Pers. Soc. Psychol. 86, 112–129.

Polderman, T.J.C., Stins, J.F., Posthuma, D., Gosso, M.F., Verhulst, F.C., & Boomsma, D.I., 2006. The phenotypic and genotypic relation between working memory speed and capacity. Intelligence 34, 549–560.

Rubinov, M., & Sporns, O., 2010. Complex network measures of brain connectivity: uses and interpretations. NeuroImage 52, 1059–1069.

Salvador, R., Suckling, J., Schwarzbauer, C., & Bullmore, E., 2005. Undirected graphs of frequency-dependent functional connectivity in whole brain networks. Philos. Trans. R. Soc. Lond. B Biol. Sci. 360, 937–946.

Smit, D.J., Stam, C.J., Posthuma, D., Boomsma, D.I., & de Geus, E.J., 2008. Heritability of "small-world" networks in the brain: a graph theoretical analysis of resting-state EEG functional connectivity. Hum. Brain Mapp. 29, 1368–1378.

Smith, S.M., Fox, P.T., Miller, K.L., Glahn, D.C., Fox, P.M., Mackay, C.E., Filippini, N., Watkins, K.E., Toro, R., Laird, A.R., & Beckmann, C.F., 2009. Correspondence of the brain's functional architecture during activation and rest. Proc. Natl. Acad. Sci. U. S. A. 106, 13040–13045.

Stam, C.J., & Reijneveld, J.C., 2007. Graph theoretical analysis of complex networks in the brain. Nonlinear Biomed. Phys. 1, 3.

Stevens, A.A., Tappon, S.C., Garg, A., & Fair, D.A., 2012. Functional brain network modularity captures inter- and intra-individual variation in working memory capacity. PLoS One 7, e30468.

Tzourio-Mazoyer, N., Landeau, B., Papathanassiou, D., Crivello, F., Etard, O., Delcroix, N., Mazoyer, B., & Joliot, M., 2002. Automated anatomical labeling of activations in SPM using a macroscopic anatomical parcellation of the MNI MRI single-subject brain. NeuroImage 15, 273–289.

van den Heuvel, M.P., & Sporns, O., 2011. Rich-club organization of the human connectome. J. Neurosci. 31, 15775–15786.

van den Heuvel, M.P., Stam, C.J., Boersma, M., & Hulshoff Pol, H.E., 2008. Small-world and scale-free organization of voxel-based resting-state functional connectivity in the human brain. NeuroImage 43, 528–539.

van den Heuvel, M.P., Stam, C.J., Kahn, R.S., & Hulshoff Pol, H.E., 2009. Efficiency of functional brain networks and intellectual performance. J. Neurosci. 29, 7619–7624.

van den Heuvel, M.P., van Soelen, I.L., Stam, C.J., Kahn, R.S., Boomsma, D.I., & Hulshoff Pol, H.E., 2013. Genetic control of functional brain network efficiency in children. Eur. Neuropsychopharmacol. 23, 19–23.

Van Dijk, K.R., Sabuncu, M.R., & Buckner, R.L., 2012. The influence of head motion on intrinsic functional connectivity MRI. NeuroImage 59, 431–438.

van Wijk, B.C., Stam, C.J., & Daffertshofer, A., 2010. Comparing brain networks of different size and connectivity density using graph theory. PLoS One 5, e13701.

Wang, J., Zuo, X., & He, Y., 2010. Graph-based network analysis of resting-state functional MRI. Front. Syst. Neurosci. 4, 16.

Watts, D.J., & Strogatz, S.H., 1998. Collective dynamics of 'small-world' networks. Nature 393, 440–442.

Wright, M.J., & Martin, N.G., 2004. Brisbane Adolescent Twin Study: Outline of study methods and research projects. Aust. J. Psychol. 56, 65–78.

Xia, M., Wang, J., & He, Y., 2013. BrainNet Viewer: a network visualization tool for human brain connectomics. PLoS One 8, e68910.